AGU PUBLICATIONS

JGR

Journal of Geophysical Research: Solid Earth

RESEARCH ARTICLE

10.1002/2016JB013789

Key Points:
- Magnetic inclinations recorded in the studied speleothem are biased by the slope of the speleothem surface
- Magnetic inclination is controlled by the ambient magnetic field but hence influenced by particle rolling down the speleothem surface
- We suggest that future studies of paleomagnetism in speleothems only consider data obtained from horizontal calcite layers

Correspondence to:
J. M. Ponte,
jorgeponte89@gmail.com

Citation:
Ponte, J. M., E. Font, C. Veiga-Pires, C. Hillaire-Marcel, and B. Ghaleb (2017), The effect of speleothem surface slope on the remanent magnetic inclination, *J. Geophys. Res. Solid Earth*, *122*, doi:10.1002/2016JB013789.

Received 24 NOV 2016
Accepted 13 JUN 2017
Accepted article online 15 JUN 2017

The effect of speleothem surface slope on the remanent magnetic inclination

J. M. Ponte[1], E. Font[1], C. Veiga-Pires[2], C. Hillaire-Marcel[3], and B. Ghaleb[3]

[1]Instituto Dom Luiz, Faculdade de Ciências, Universidade de Lisboa, Lisboa, Portugal, [2]CIMA-FCT, Universidade do Algarve, Faro, Portugal, [3]GEOTOP, Université du Québec, Montreal, Canada

Abstract Speleothems are of interest for high-resolution reconstruction of the Earth's magnetic field. However, little is known about the influence of speleothem morphologies on their natural remanent magnetization (NRM) record. Here we report on a high-resolution paleomagnetic study of a dome-shaped speleothem of middle Holocene age from southern Portugal, with special attention to the anisotropy of magnetic susceptibility (AMS) and anisotropy of anhysteretic remanent magnetization (AARM). To assess the potential influence of the slope of the speleothem surface on the recorded remanent magnetization, we compare magnetic directions and AMS and AARM fabrics from subhorizontal to gradually subvertical calcite growth layers collected in a transversal cross section of the speleothem. A linear correlation is observed between magnetic inclinations, calcite laminae slope, and AARM k_1 inclination. The AMS fabric is mostly controlled by calcite crystals, with direction of the minimum axes (k_3) perpendicular to laminae growth. Magnetic inclinations recorded in inclined and vertical calcite growth layers are underestimated when compared to a global paleosecular variation (PSV) model. After extrapolating magnetic inclinations to the horizontal, the corrected data better fit the PSV model but are still lower than the predicted magnetic inclinations, suggesting that inclination shallowing affects the entire speleothem. We suggest that speleothem morphology exerts a critical role on the magnetic inclination recording, which is controlled by the Earth's magnetic field but also influenced by particle rolling along the sloping surfaces. These observations open new avenues for reconstructing high-resolution paleomagnetic secular variation records from speleothems and provide new insights into their NRM acquisition mechanisms.

1. Introduction

Speleothems are high-resolution archives of the Earth's climate and the intensity of its magnetic field [*Latham et al.*, 1979; *Morinaga et al.*, 1986; *Martin*, 1990; *Lascu and Feinberg*, 2011; *Osete et al.*, 2012; *Strauss et al.*, 2013; *Font et al.*, 2014; *Bourne et al.*, 2015; *Jaqueto et al.*, 2016; *Lascu et al.*, 2016]. However, little is known about the influence of the slope of calcite growth layers of speleothems on the orientation of recorded natural remanent magnetization (NRM). Pioneer paleomagnetic studies suggested that the difference of the magnetic inclination recorded along the speleothem surface is not large enough to assess whether they are due to the slope or to the measurement error [e.g., *Latham et al.*, 1982, 1986, 1989; *Morinaga et al.*, 1989; *Lean et al.*, 1995; *Openshaw et al.*, 1997]. More recently, *Zhu et al.* [2012] applied anisotropy of magnetic susceptibility (AMS) and anisotropy of isothermal remanent magnetization techniques to two speleothems and concluded that the orientation of ferrimagnetic minerals in speleothems are not controlled by the speleothem growth laminae but by the geomagnetic field. To unravel the potential effect of the speleothem's morphology on the recorded NRM vector directions, it is therefore useful to consider the variation of the direction of the primary (detrital) magnetization along a speleothem at a high temporal/spatial resolution. This is not straightforward because speleothems generally contain very low amounts of magnetic particles within the diamagnetic calcite matrix. Such a limitation can be solved by using large ($2 \times 2 \times 2$ cm) paleomagnetic samples. However, taking into account that the thickness of annual lamination is generally of a millimetrical scale, this solution results in a low temporal resolution.

The aim of this study is to examine the potential influence of calcite growth patterns on the NRM directions using a well-dated, high growth rate mid-Holocene speleothem (~3200–4500 years B.C.) collected from the Algarve region, in southern Portugal. This speleothem, already studied by *Font et al.* [2014], carries a primary (detrital) remanent magnetization due to detrital magnetite and maghemite and exhibits high values of remanent magnetization of the order of 10^{-3} A/m. Such properties allowed us to collect relatively small

specimens but with a high temporal and spatial resolution. Detailed U-Th measurements [*Ghaleb et al.*, 2014] provided a robust age model, using StalAge algorithm for interpolations [*Scholz and Hoffmann*, 2011]. On these grounds, paleomagnetic data could be compared with a reference model of paleosecular variations.

2. Geological Setting and Sampling

The karst system investigated is developed in Jurassic limestones from the sedimentary sequence of the Algarve basin, southern Portugal. These consist of reef and bioclastic carbonates capped by Terra Rossa soils. Laterally, the limestones are replaced by a nearshore facies with either silex nodule layers or sandstones with siliceous-fossil-rich pockets [*Terrinha et al.*, 2013]. The SPA speleothem was collected in the *Excentricas Cave* (geographic coordinates of 37°06′ N, 7°46′W), located over the large Peral-Moncarapacho karstic aquifer of Algarve, Southern Portugal. The *Excentricas cave* lies over the Querença-Silves aquifer system (Cerro da Cabeça). The region is dominated by a Mediterranean climate with a mean annual precipitation below 500 mm generally falling in autumn and spring and a mean annual temperature of 18°C. The area depicts a scrubland vegetation cover with sparse shrubs and small trees (*Querqus coccifera*, *Ilex aquifolium*, etc).

The studied speleothem shows parallel banding, with no layer showing anomalous detrital mineral accumulation or even dissolution, suggesting that growth was almost continuous along the studied profile. The speleothem has also a peculiar shape, because the growth layers do not become thinner and condensed along the sides of the speleothem (Figure 1a). It corresponds to a dripstone with a conical shape and tapered form, similar to a mammiform speleothem [*Hill and Forti*, 1997]. Detailed mineralogical data, magnetic properties, and carbon and oxygen isotopic compositions from a portion of the speleothem under study (named SPAII) are documented in *Font et al.* [2014].

Subsampling for U-Th dating was achieved on a 1 cm thick slice cut along the growth axis of the stalagmite. For paleomagnetic analysis, the sampled section of the speleothem was thoroughly oriented using a magnetic compass. As illustrated by Figure 1a, the strike and dip of the vertical section are N80° and 90°, respectively. Small cylindrical specimens of approximately 2 cm^3 in volume (1.1 cm in diameter and 2 cm in length) were subsequently drilled in the laboratory perpendicularly to the oriented face of the speleothem and named SPAIV (Figure 1b) (samples SPAIII being the focus of another study). The orientation of the specimens was reported by a vertical line pointing to the top of the cylinder as illustrated in Figures 1c and 1d. The final declination value of the cylindrical specimens is N168°, considering a correction of the local declination of $\sim -2°$ (N80° + 90° − 2°), with a dip of 0°. Specimens were collected from the top of the speleothem (where calcite laminae are inclined to subhorizontal) to the laterally strongly dipping calcite growth layers (Figure 1b). A total of six horizons or "lines" (called SPAIV.3-5-7-9-11-13; Figure 1) were selected, each one recording a specific time span, leading to a total of 48 samples (8 samples per line; Figure 1b).

3. Methods

The U-series measurements for age determination were performed at the Radiochronology laboratory of the GEOTOPO-UQAM-McGill research Center, Canada. Each half or centimeter-thick subsample of about 2 to 4 g was grinded in an agate mortar for subsequent U-series isotope measurements. The sample powders were dissolved using nitric acid in a Teflon™ beaker into which a weighted amount of calibrated mixed spike ^{233}U-^{236}U-^{229}Th had been placed and evaporated slowly to dryness. After the dissolution around 10 mg of iron carrier was added and the solution was then left over night for spike-sample equilibration. U and Th were coprecipitated with $Fe(OH)_3$ by adding ammonium hydroxide drop by drop until reaching pH 8–9. The precipitate was recovered by centrifugation and washed twice with deionized water, then dissolved in 6 N HCl. U-Th separation was performed on a 2 mL AG1X8 anionic resin volume. The thorium fraction was recovered though elution with 6 N HCl, and the U and Fe fraction, with water. The U fraction was purified on a 0.2 mL U-Teva™ (Elchrom industry™) resin volume. Fe was eluted with 3 N HNO_3 and the U fraction with 0.02 N HNO_3. After drying, thorium purification was carried out on a 2 mL AG1X8 resin in 7 N HNO_3 and eluted with 6 N HCl. U-Th measurements were performed using a multicollector inductively coupled plasma mass spectrometry Nu instrument ™. ^{236}U-^{235}U-^{234} U-^{233} U and ^{232}Th-^{230}Th-^{229}Th were measured on the ion counter (IC0) in peak switching mode for uranium and thorium isotopes, respectively. ^{238}U was not measured but calculated from ^{235}U/^{236}U ratios, assuming a constant ^{238}U/^{235}U mass ratio (137.88). Knowing ^{236}U/^{233}U of the spike, mass bias corrections in atomic mass unit (amu^{-1}) were calculated and used to correct measured ratios

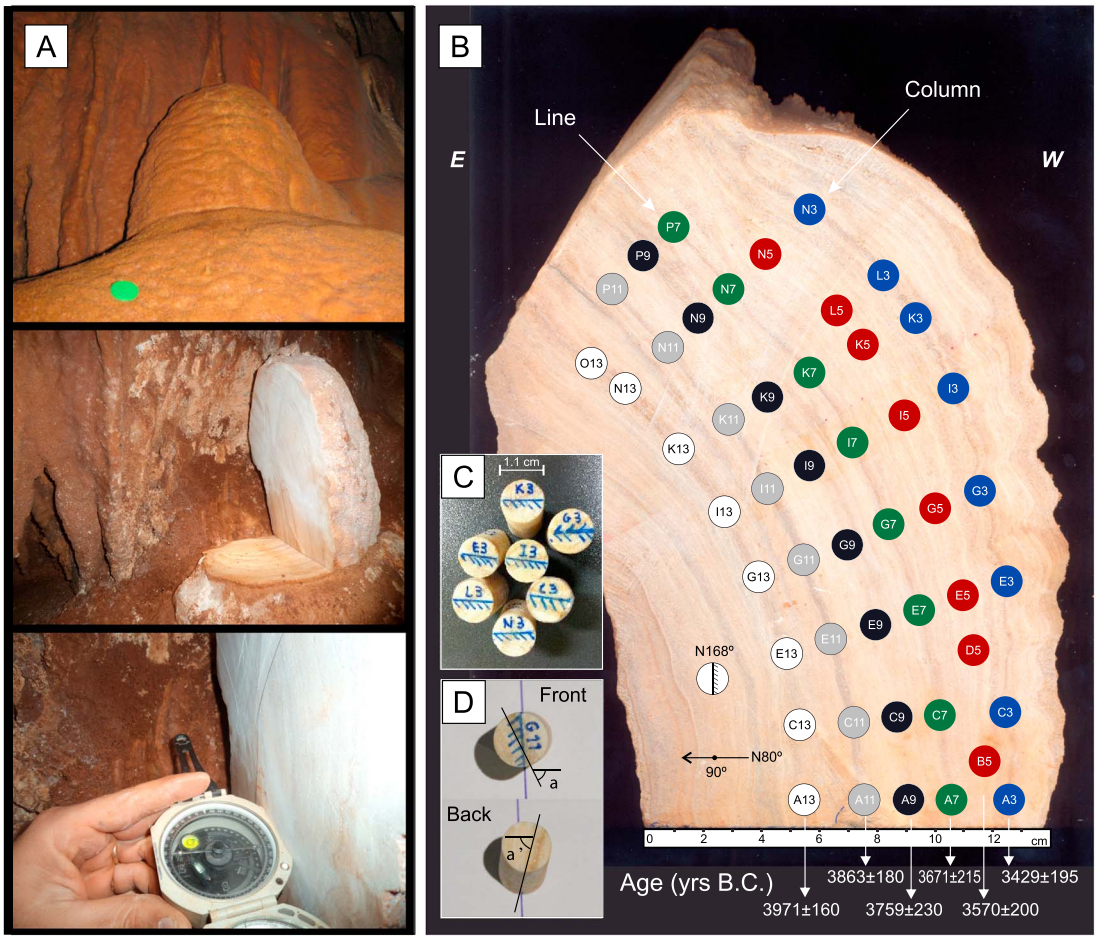

Figure 1. (a) Photographs of speleothem under study before cutting (top), after cutting and replacement in its original position (middle), and orientation of the vertical plane with a magnetic compass (bottom). (b) Vertical face of the speleothem with location of the cylindrical SPAIV specimens (1.1 × ~2 cm) collected for subsequent paleomagnetic measurements. Samples are distributed along lines corresponding to calcite growth layers of a similar age, and columns that represent the temporal variations. Each line includes a reference calcite growth layer (darker). Ages Before Christ (B.C.) and associated errors have been determined by interpolation of corrected ^{230}Th ages for dated layers using the StalAge algorithm [*Scholz and Hoffmann*, 2011]. (c) Cylindrical specimens and their respective orientation illustrated in Figure 1b. (d) The dip of calcite laminae is calculated based on the mean of the angles measured on the front (α) and back sides (α') of the specimen.

between uranium isotopes and between thorium isotopes. In order to get a direct insight into isotopic properties of contaminating detrital fractions eventually transported into the cave and incorporated into speleothem calcite layers, clay fractions (<2 μm) from soils overlying the karts system (Terra Rossa) were sampled and pooled. The above U-Th chemical extraction procedures were used for the clay fraction, except at early sample dissolution stage, for which we used a mixture of concentrated HF and HNO_3. After total evaporation, 2 mL of HCl supersaturated with H_3BO_4 were added, and the solution was evaporated to dryness, prior to re-dissolution with HCl 6 M. The overall analytical reproducibility was estimated from replicate measurement of a uraninite standard Hu-1. Precision is usually better than ±0.5% for uranium results and around 1% for thorium in young samples at two sigma levels.

Finally, detrital values of U/Th ratio determined from Terra Rossa soils and the stratigraphical ordering of samples as proposed by *Hellstrom* [2006] similarly corrected ^{230}Th ages. One of the layers was also sampled several times for the setting of an isochron age also in accordance with other correction methods [*Ghaleb et al.*, 2014]. Model ages of the six lines of samples were finally estimated by interporlation between corrected ^{230}Th ages and using the algorithm StalAge [*Scholz and Hoffmann*, 2011] (Figure 2).

Magnetic measurements were performed at the Paleomagnetism Laboratory of the Instituto Dom Luis, Faculty of Sciences of the University of Lisbon, Portugal. The magnetic remanence was measured using a JR6 spinner magnetometer (sensitivity of 2.4 × 10^{-6} A/m) after stepwise alternating field

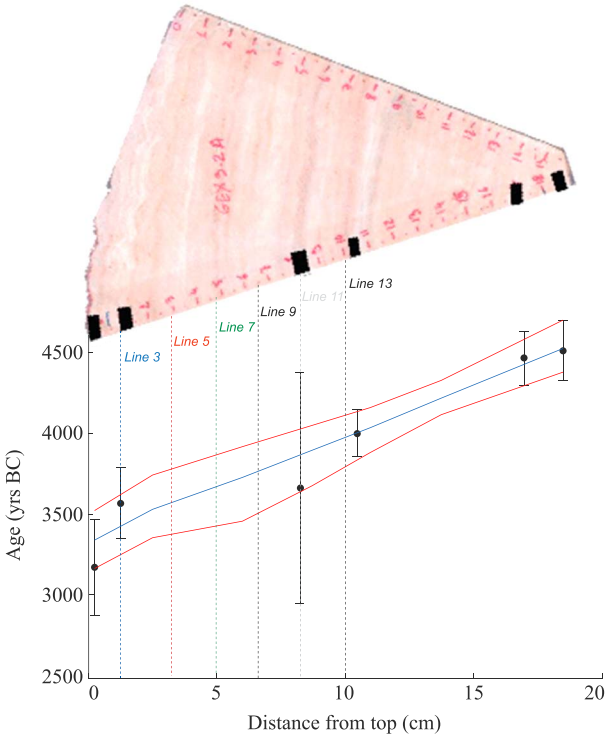

Figure 2. Age model for SPAIV obtained from the StalAge algorithm [*Scholz and Hoffmann*, 2011]. The blue and red lines represent the estimated ages and their upper and lower 95% confidence limits, respectively. The vertical dashed lines correspond to each sample line (see Figure 1). The black points represent the input data as corrected ^{230}Th ages and their respective errors.

(AF) demagnetisation using a tumbling LDA-3A demagnetizer device. Characteristic remanent magnetization (ChRM) was calculated based on principal component analysis [*Kirschvink*, 1980] and Fisher statistics [*Fisher*, 1953] using the software Remasoft 6.0 (AGICO) software.

Low field anisotropy of magnetic susceptibility (AMS) was measured with a MFK1-FA Kappabridge (AGICO), with a field of 200 A/m and a frequency of 976 Hz. Data were analyzed by using the Anisoft 4.2 software of AGICO. The magnetic anisotropy is represented by an ellipsoid whose geometry is given by its principal axes, or eigenvectors K_{max} (k_1) $\geq$ K_{inter} (k_2) $\geq$ K_{min} (k_3) of the corresponding AMS tensor [*Tarling and Hrouda*, 1993]. The susceptibility difference ΔK ($\Delta K = k_1 - k_3$) and the shape parameter U ($U = (2\ k_2 - k_1 - k_3)/(k_1 - k_3)$) [*Jelinek*, 1981] are preferentially used for samples having very low or negative values of magnetic susceptibility [*Hrouda*, 1986; *Hirt and Almqvist*, 2012].

Anisotropy of anhysteretic remanent magnetization (AARM) was performed following the method of *McCabe et al.* [1985]. This technique is useful for sedimentary rocks that have low (or negative) bulk susceptibility values, as in this case, and isolates the contribution of the ferromagnetic minerals. AARM is obtained by a combination of a DC magnetic field of 0.5 mT and an alternating field (AF) magnetic field of 50 mT. Samples were previously demagnetized using AF of 50 mT using a LDA-3A demagnetizer. Remanence was measured with the JR6 spinner magnetometer. The procedure was repeated for six different orientations, and data were treated using the software Anisoft 4.2 (AGICO). AARM is represented by an ellipsoid defined by the three principal axes (minimum, intermediate, and maximum susceptibility axes). The anisotropy degree is evaluated by the P parameter ($P = k_1/k_3$), and the shape is defined by the T parameter ($T = 2\ (\ln(k_2) - \ln(k_3))/(\ln(k_1) - \ln(k_3)) - 1$).

Slopes (dips) of calcite growth layers versus the horizontal plane were calculated based on the mean between the angles measured on the front and the back faces of each cylindrical sample as illustrated by Figure 1d.

The coefficient of determination R^2 has been determined using the most general definition, $R^2 = 1 - (SS_{residual}/SS_{total})$, where SS_{total} is the total sum of squares and $SS_{residual}$ is the sum of squares of residuals.

4. Results

4.1. U-Th Dating and Age Model

The studied speleothem was first analyzed for its ^{14}C content. Result yielded conventional ages ranging from 6048 ± 45 to 4836 ± 47 years (±1σ) [*Veiga-Pires et al.*, 2011]. However, since cave $^{14}CO_2$ offsets with atmospheric CO_2 are not known and might have varied through time, U-series measurements were made in order to obtain ^{230}Th ages. The precise U-series dating of this speleothem revealed to be challenging, due to its low total U-content (mean ~ 115 ppb) and relatively abundant contaminating detrital fraction, illustrated by a mean ^{232}Th content of ~12 ppb. Several corrections have been proposed in literature in order to estimate

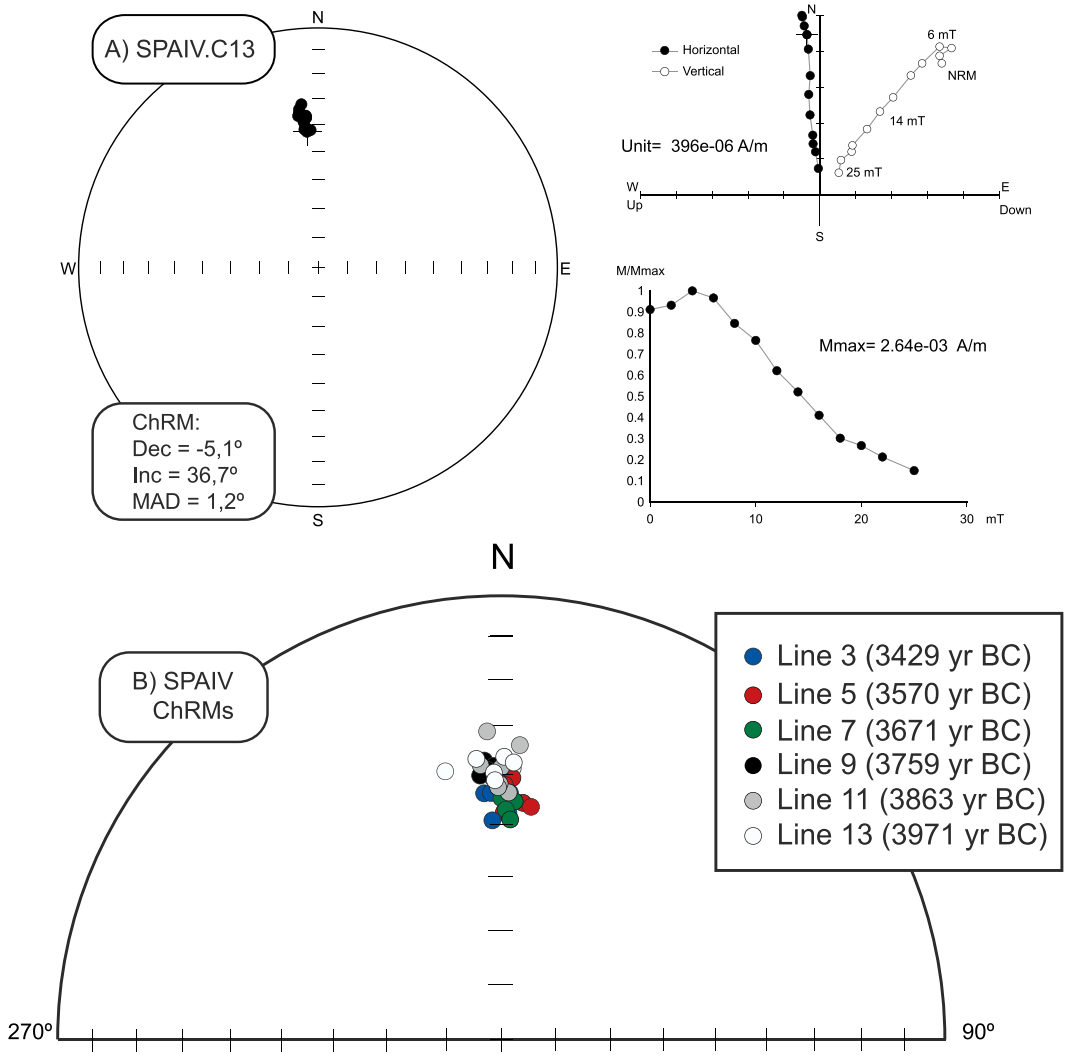

Figure 3. (a) Stereographic and orthogonal projections and remanence intensities during alternating field (AF) cleaning of sample SPAIV_C13. After cleaning a viscous remanent magnetization below 6 mT, the orthogonal projection shows a unidirectional magnetic vector pointing to the origin. (b) Stereographic projections of the characteristic remanent magnetizations (ChRMs) obtained from all specimens; the colors correspond to the different lines.

the U strictly coprecipitated within calcite and its in-grown daughter ^{230}Th isotope, to be used for calculating sample ages. The isotopic composition of the contaminating fraction is generally considered uniform in U-Th dated speleothems or, at least, within given growth layers, and estimated from ^{232}Th-contents strictly inherited with this fraction. The detrital-source isotopes are quantified (i) assuming a mean crustal isotopic composition (i.e., [Th]/[U] ~ 3.8), or (ii) through the calculation of theoretical isotopic ratios yielding stratigraphically ordered corrected ages, or (iii) based on the isotopic composition of clay fractions in soils overlying the karst system or (iv) using an isochron approach. All methods yielded compatible results within standard deviations, the latter three with more precise final age estimates. They range from 4.52 ± 0.19 ka (bottom) to 3.08 ± 0.24 (top) ka (Figure 2). These corrected ages were then used as input values into the StalAge algorithm developed especially for determining age models in speleothems [*Scholz and Hoffmann*, 2011]. The resulting age model (Figure 2) was used to attribute an age (with given uncertainty) to each of the studied lines (Figure 1b).

4.2. Paleomagnetism

Paleomagnetic results are summarized in Figure 3 and in Table 1. NRM intensities are relatively high and range between 0.88×10^{-3} and 2.98×10^{-3} A/m, in agreement with previous data [*Font et al.*, 2014]. After

Table 1. Paleomagnetic, AMS, and AARM Data[a]

							AMS				AARM			
Specimen	Calcite Layer dip (deg)	NRM (A/m)	Dec (deg)	Inc (deg)	MAD (deg)	AF Demag. Steps	K_m (SI)	ΔK	U	k_3 (deg)	K_m (SI)	P	T	k_1 (deg)
SPAIV_A3	90	2.76E − 03	−4	43.7	1.8	7 [8, 20]	5.24E − 06	7.44E − 07	0.189	9	7.03E − 05	1.034	0.116	42
SPAIV_C3	88.5	2.33E − 03	−2.4	43.7	1.7	7 [8, 20]	3.93E − 06	9.53E − 07	0.63	6	7.20E − 05	1.045	−0.237	7.8
SPAIV_E3	79.5	2.04E − 03	2	43.7	2.5	7 [6, 18]	2.23E − 06	7.96E − 07	0.739	15	5.85E − 05	1.036	0.306	59.3
SPAIV_G3	77	2.49E − 03	0.6	44.6	1.8	6 [8, 18]	4.53E − 06	8.38E − 07	0.435	20	7.17E − 05	1.027	−0.077	7.8
SPAIV_I3	66	1.60E − 03	0.9	45.9	1.3	8 [6, 20]	7.08E − 07	8.27E − 07	0.936	31	5.15E − 05	1.037	−0.026	44
SPAIV_K3	56	2.01E-03	1.4	47.4	0.8	7 [10, 22]	1.49E − 06	9.31E − 07	0.903	41	5.89E − 05	1.03	−0.378	57.6
SPAIV_L3	48.5	1.76E − 03	1.8	47.7	1.4	8 [8, 22]	−1.09E − 06	6.57E − 07	0.945	48	5.12E − 05	1.056	0.535	42.5
SPAIV_N3	35.5	1.66E − 03	−2.3	49.1	2	8 [4, 18]	3.76E − 06	1.43E − 06	0.515	61	6.88E − 05	1.047	−0.437	54.6
SPAIV_B5	77	1.11E − 03	−2.8	40.3	3.7	5 [4, 12]	–	–	–	–	3.22E − 05	1.055	−0.547	48.7
SPAIV_D5	81.5	1.27E − 03	3.7	41.2	2	6 [6, 16]	−4.63E − 06	1.44E − 06	0.514	14	3.26E − 05	1.047	−0.366	45
SPAIV_E5	72.5	1.33E − 03	-0.3	42.3	1.5	7 [6, 18]	−7.32E − 06	1.27E − 06	0.725	23	3.56E − 05	1.06	−0.594	64.3
SPAIV_G5	75	9,90E − 04	1.1	42.1	2	5 [8, 16]	−9.18E − 06	1.09E − 06	0.79	28	2.94E − 05	1.013	−0.562	62.4
SPAIV_I5	65.5	1.19E − 03	-0.1	44.1	2.2	7 [8, 20]	−7.26E − 06	1.24E − 06	0.919	27	5.28E − 05	1.039	0.064	76.7
SPAIV_K5	52.5	9.69E − 04	0.4	48.4	2.1	6 [6, 16]	−7.95E − 06	1.05E − 06	0.696	37	3.11E − 05	1.093	−0.396	85.7
SPAIV_L5	53.5	9.49E − 04	0.8	46.2	2.3	6 [6, 16]	−8.31E − 06	1.14E − 06	0.562	44	2.83E − 05	1.074	−0.135	55.1
SPAIV_N5	43	8.81E − 04	7.3	46.1	1.7	5 [8, 16]	−8.96E − 06	1.73E − 06	0.37	47	2.84E − 05	1.072	−0.315	57.5
SPAIV_A7	87	2.08E − 03	1.7	44	2.5	8 [6, 20]	9.44E − 08	2.29E − 07	0.451	6	5.14E − 05	1.054	−0.051	80.4
SPAIV_C7	85	1.82E − 03	0.3	43.6	2.4	8 [6, 20]	9.69E − 06	1.55E − 06	0.357	7	4.61E − 05	1.036	−0.376	63
SPAIV_E7	70.5	1.91E − 03	0	44.4	1	8 [6, 20]	−7.16E − 07	1.21E − 06	0.249	20	5.00E − 05	1.04	−0.616	39.8
SPAIV_G7	71	1.88E − 03	0	44.2	1.9	8 [6, 20]	1.76E − 06	1.15E − 06	0.281	23	4.40E − 05	1.067	−0.088	28.1
SPAIV_I7	62.5	1.88E − 03	3.5	45.1	1.8	8 [6, 20]	2.08E − 06	8.66E − 07	0.66	34	4.92E − 05	1.063	−0.4	62.4
SPAIV_K7	49	1.87E − 03	0.9	46.5	1.7	8 [4, 18]	−1.01E − 06	8.85E − 07	0.88	41	5.31E − 05	1.044	−0.725	62.6
SPAIV_N7	51	2.00E − 03	0.7	46.4	1.9	8 [6, 20]	5.18E − 06	9.02E − 07	0.079	42	6.34E − 05	1.058	−0.482	59.8
SPAIV_P7	34	2.03E − 03	2.4	48.7	1.7	8 [6, 20]	4.50E − 06	1.20E − 06	0.003	58	6.65E − 05	1.054	−0.072	58.2
SPAIV_A9	88	1.30E − 03	−3.5	37.1	2.4	7 [6, 18]	−1.97E − 06	5.18E − 07	0.924	16	3.38E − 05	1.054	0.15	57.8
SPAIV_C9	86	1.28E − 03	0.3	38.9	1.9	7 [6, 18]	−4.52E − 06	9.13E − 07	0.415	14	3.72E − 05	1.057	−0.067	27.4
SPAIV_E9	65	1.19E − 03	−1.6	38.3	2.1	7 [6, 18]	−5.37E − 06	9.13E − 07	0.63	27	3.43E − 05	1.171	0.445	48.1
SPAIV_G9	70	1.18E − 03	−3	39	1.8	7 [6, 18]	−5.58E − 06	8.78E − 07	0.814	26	3.26E − 05	1.037	−0.524	41.3
SPAIV_I9	61.5	1.32E − 03	−2.1	40.4	1.7	7 [6, 18]	−5.25E − 06	1.01E − 06	0.768	36	3.72E − 05	1.042	−0.253	38.3
SPAIV_K9	51	1.60E − 03	−4.6	40	2.2	7 [6, 18]	−3.48E − 06	1.14E − 06	0.658	50	4.62E − 05	1.071	0.089	68.9
SPAIV_N9	54.5	1.16E − 03	0.8	41.8	2.2	6 [6, 16]	−4.81E − 06	7.63E − 07	0.839	50	3.89E − 05	1.059	−0.592	54.2
SPAIV_P9	35	9.99E − 04	−2.5	44.7	2.4	6 [6, 16]	−2.72E − 06	6.30E − 07	0.795	61	4.24E − 05	1.067	−0.265	68.4
SPAIV_A11	84	1.05E − 03	−2.5	31.4	3	8 [6, 20]	3.38E − 05	1.09E − 06	0.67	12	6.06E − 05	1.047	0.106	17.1
SPAIV_C11	76.5	1.65E − 03	−4.3	38	2.7	7 [8, 20]	3.61E − 05	1.15E − 06	0.714	15	7.72E − 05	1.061	−0.243	67.2
SPAIV_E11	68.5	1.45E − 03	0.1	39.8	1.4	7 [6, 18]	2.90E − 06	8.44E − 07	0.697	25	6.88E − 05	1.064	0.67	13
SPAIV_G11	70.5	1.66E − 03	3.6	34	3.5	7 [4, 16]	3.79E − 06	7.89E − 07	0.849	27	7.29E − 05	1.055	−0.287	39.7
SPAIV_I11	60	1.60E − 03	−1.6	40.8	1.6	7 [6, 18]	4.19E − 06	1.22E − 06	0.077	29	8.53E − 05	1.055	−0.654	50.3
SPAIV_K11	51	1.51E − 03	1.7	43.6	2.6	6 [8, 18]	4.88E − 06	9.94E − 07	0.867	44	8.31E − 05	1.037	−0.486	47.1
SPAIV_N11	50.5	1.80E − 03	-0.4	41.9	2	7 [6, 18]	7.63E − 06	9.14E − 07	0.771	45	9.49E − 05	1.072	0.274	38.5
SPAIV_P11	33.5	2.28E − 03	-0.7	42.6	2.9	6 [6, 16]	2.31E − 05	5.59E − 07	0.549	64	1.54E − 04	1.099	−0.249	67.5
SPAIV_A13	87.75	1.71E − 03	−11.8	38.3	3.2	5 [12, 20]	8.58E − 06	1.34E − 06	0.561	11	8.61E − 05	1.038	0.553	4.5
SPAIV_C13	76.5	2.64E − 03	−5.1	36.7	1.2	7 [8, 20]	8.22E − 06	1.20E − 06	0.605	23	9.11E − 05	1.071	−0.162	62.3
SPAIV_E13	72	2.87E − 03	0.7	36.1	2.1	8 [6, 20]	6.55E − 06	1.45E − 06	0.924	28	8.63E − 05	1.073	0.137	19
SPAIV_G13	69.5	2.89E − 03	2.6	37.6	1.5	8 [6, 20]	6.57E − 06	1.06E − 06	0.719	27	8.12E − 05	1.114	−0.313	35.9
SPAIV_I13	62	2.37E − 03	2.5	38.5	2.3	8 [6, 20]	4.77E − 06	1.25E − 06	0.521	31	7.49E − 05	1.101	−0.745	54.5
SPAIV_K13	47	2.19E − 03	−2.6	39.4	2.2	8 [6, 20]	3.27E − 06	2.28E − 06	0.263	49	7.50E − 05	1.067	−0.778	69.4
SPAIV_N13	41	2.98E − 03	−1.5	41.3	1.6	8 [6, 20]	6.44E − 06	1.31E − 06	0.714	49	7.92E − 05	1.07	−0.256	55.8
SPAIV_O13	37	2.31E − 03	−4.4	42.2	2.1	6 [6, 16]	–	–		–	6.55E − 05	1.06	0.065	77.3

[a]Dec. and Inc. represent the magnetic declination and inclination respectively; MAD is the maximum angular deviation; NRM is the natural remanent magnetization intensity; K_m is the mean magnetic susceptibility; ΔK is the susceptibility difference and U corresponds to the shape anisotropy parameter obtained from AMS measurement; P and T correspond to anisotropy degree and shape parameters, respectively; and inclination of k_3 (AMS) and k_1 (ARM) axes are also indicated.

AGU Journal of Geophysical Research: Solid Earth

10.1002/2016JB013789

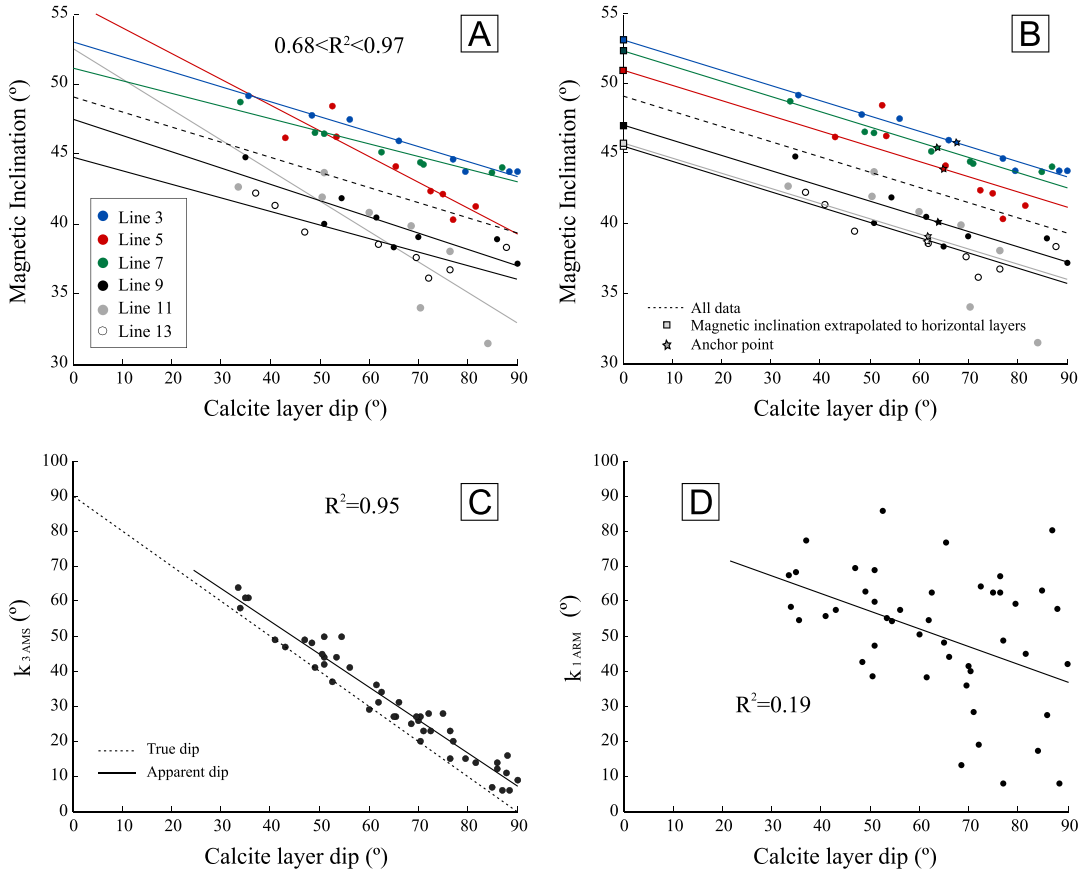

Figure 4. (a) Remanent magnetic inclination as a function of the calcite layer dip. The dashed line represents the linear regression considering all data. (b) Same data but with the trend line corrected by using the slope of the linear regression calculated in Figure 4a. The anchor points (stars) are defined by the sample based mean magnetic inclination and the mean calcite layer dip of each line. Extrapolated magnetic inclinations for horizontal calcite layer are obtained at calcite dip = 0°. (c) k_{3AMS} and (d) k_{1ARM} inclinations in function of the calcite layer dip. The determination coefficient ($R^2 = 1 - (SS_{residual}/SS_{total})$) is also shown.

cleaning of a weak (viscous) magnetization below 6 to 8 mT, orthogonal projections show stable and well-defined remanent magnetization directions trending to the origin (Figure 3a). After AF demagnetization at 25 mT, about 90% of the remanence was cleaned. The median destructive field ranges between 10 and 15 mT, confirming the presence of a low coercive phase (magnetite) as previously described by *Font et al.* [2014]. Sample-based magnetic directions are well clustered within a region from 348.2° to 5.2° in declination and from 31.4° up to 49.1° in inclination (Figure 3b). Maximum angle deviation (MAD) values are low (0.8° to 3.7°). The recorded magnetic inclinations decrease from the top to the base of the speleothem, a pattern verified in all six lines (Figure 4a) and evidenced by the striking correlations ($0.67 < R^2 < 0.97$) between the magnetic inclination and the dip angle of the corresponding calcite laminae. The trend is very similar in four of the studied lines (3, 7, 9, and 13) and slightly higher in lines 5 and 11.

4.3. Anisotropy of Magnetic Susceptibility

The AMS data are illustrated in Figure 5 and in Table 1. The bulk susceptibility ($K_m = [k_1 + k_2 + k_3]/3$) varies from -9.18×10^{-6} to 3.61×10^{-5} (SI) and includes 18 samples with negative values and 28 samples with positive values (Figure 5a). These values are slightly higher than the magnetic susceptibility of pure calcite ($K_m = -12.1 \times 10^{-6}$ SI [*Schmidt et al.*, 2006] or $K_m = -15 \times 10^{-6}$ SI [*Borradaile and Jackson*, 2010]), pointing toward a major contribution of diamagnetism due to calcite and a few, but significant, contribution of paramagnetic and/or ferromagnetic minerals to the bulk susceptibility.

The AMS eigenvectors ($k_1 \geq k_2 \geq k_3$) are clustered within elongate 95% confidence regions (Figure 5b). Parameters k_1 and k_2 are confined within an NW-SE great circle, while k_3 is oriented NE-SW and has inclination values ranging from nearly horizontal to 70° (Figure 5b).

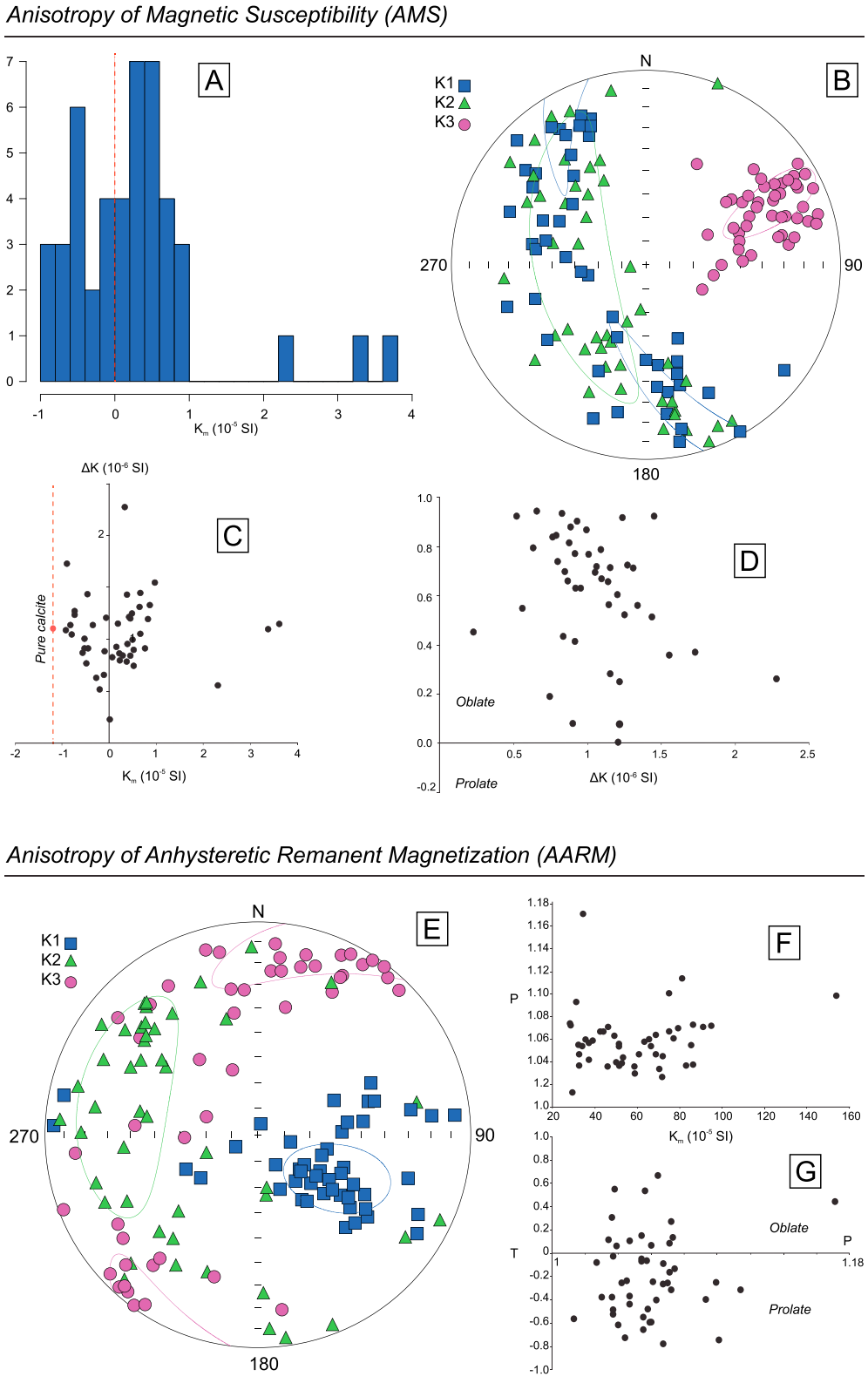

Figure 5. AMS and AARM data of the SPAIV speleothem. (a) Histogram of the mean magnetic susceptibility. (b) Representation of the three principal axis of magnetic susceptibility: k_1 (squares), k_2 (triangles), and k_3 (circles). (c) Susceptibility difference (ΔK) versus bulk susceptibility (K_m) diagram. The red point in ΔK-K_m represents the reference value for pure calcite [*Schmidt et al.*, 2006]. (d) Shape anisotropy (U) versus ΔK; oblate and prolate domain are also shown. (e) Representation of the three principal axis of anhysteretic magnetic remanence: k_1 (squares), k_2 (triangles), and k_3 (circles). (f) P parameter (anisotropy degree) versus bulk susceptibility diagram. (g) Shape parameter (T) versus anisotropy degree parameter (P).

The susceptibility difference ΔK varies from 2.29×10^{-7} to 2.28×10^{-6} SI (Figure 5c). The mean value of ΔK is 1.05×10^{-6} SI, comparable to the reference value of 1.1×10^{-6} SI of calcite [*Schmidt et al.*, 2006]. The U parameter is positive for all samples, confirming the oblate fabric suggested by the orientation of the AMS ellipsoid (Figure 5d).

The oblate shape and the gradually decreasing k_3 inclinations with respect to the calcite layer inclination points to a fabric that mimics the shape of the speleothem, i.e., where the magnetic foliation (k_1-k_2) is concordant with the surface of the speleothem with k_3 perpendicular to it. Such a feature is strengthened by the very strong positive correlation ($R^2 = 0.95$) between k_3 inclination and the dip of the calcite layers (Figure 4c). Samples from the base of the speleothem (vertical layers) display the highest k_3 inclinations, while the samples located at the top (subhorizontal layers) are nearly vertical. However, the inclination of the k_3 susceptibility eigenvector is systematically steeper (by over 10° in some cases) than the complement to the calcite layer dip (90°-calcite layer dip) (Figure 4c), which suggests that the measured calcite layer angle is an apparent dip rather than the true dip or that the orientation of the AMS ellipsoid is slightly influenced by the orientation of the AARM ellipsoid (i.e., orientation of the ferromagnetic particles).

The striking correlation between k_{3AMS} and the calcite layer dip suggests that a close relationship exists between the orientation of the AMS fabric and the crystallographic orientation of the calcite crystals, similarly to what has been shown by *Zhu et al.* [2012]. The crystallization of calcite crystals in speleothems follows the direction of the *c* axis, which corresponds to the longest axis perpendicular to the bedding plane. This orientation corresponds to the k_{3AMS} axes measured in this study.

4.4. Anisotropy of Anhysteretic Remanent Magnetization

AARM data are illustrated in Figure 5 and Table 1. Most of the maximum remanent anisotropy axes (k_{1ARM}) are preferentially distributed within the SE quadrant of the stereographic projection and show variable inclinations ranging from 40 to 80° (Figures 5e and 5g). The intermediate and minimum axes (k_{1ARM} and k_{2ARM}) are more dispersed but distributed along a NE-SW great circle (Figure 5e).

The samples exhibit a weak ARM anisotropy, with *P* ranging from 1.013 to 1.114, at the exception of sample E9 that shows a *P* of 1.171 (Figure 5f). Despite this low anisotropy, the fabric is a dominantly prolate (more than 70% of the samples), while some samples exhibit an oblate fabric, as shown by *T* values ranging from −0.778 to 0.670 (Figure 5g). The k_{1ARM} are not close to the horizontal plane but are rather steeply inclined (Figure 5e). More exactly, subhorizontal calcite layer has higher values of k_{1ARM} inclination (60–80°), while subvertical calcite layer exhibits shallower k_{1ARM} inclinations (Figure 4d). This suggests that the orientation of the AARM ellipsoid (i.e., orientation of the ferromagnetic particles) depend on the slope: the steeper the slope is, the shallower the k_1 axes. Interestingly, samples located at the top of the speleothem, where the slope is shallower (~35°), show a lower dispersion of the k_{1ARM} (55° to 75°) than in the case of samples located at the bottom (dip of 90°) for which k_{1ARM} ranges from 5° to 80° (Figure 4d). Such a gradual increase in the k_{1ARM} dispersion suggests that the distance traveled by ferromagnetic minerals from the top to the bottom, as the water drops travel down the speleothem's surface, has a strong influence on the orientation of the AARM ellipsoids (see below).

5. Discussion

The new paleomagnetic data presented above indicate that the main magnetic carrier of the speleothem investigated in the present study is a low coercive phase, probably corresponding to magnetite and/or maghemite. Data corroborates previous results by *Font et al.* [2014], who pointed to the presence of a primary (detrital) remanent magnetization carried by pedogenic magnetite/maghemite based on detailed rock magnetic properties and microscopic observations. In contrast to most examples from the literature, the present SPAIV speleothem has rather high NRM intensities (~10^{-3} A/m) linked to the presence of a terrigenous detrital fraction also labeled by high detrital Th contents. The speleothem under study has a peculiar curved shape, in which the thickness of the calcite laminae remains nearly constant along the growth surface. Both peculiarities provide the means to document with accuracy the influence of the speleothem shape on the recorded Earth's magnetic field.

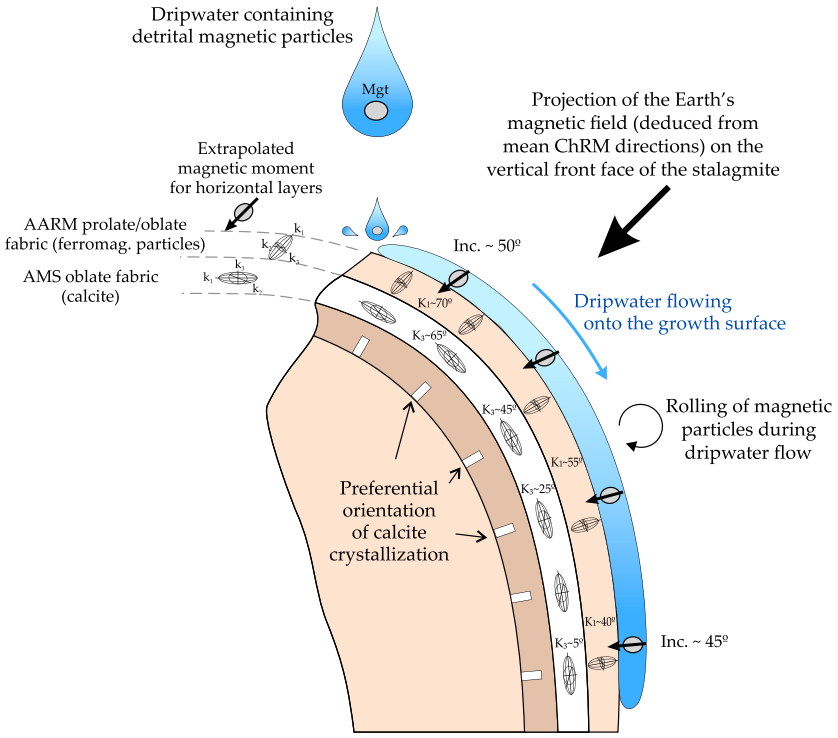

Figure 6. Conceptual model of the orientation of the magnetic grains when dripwater flows along the speleothem surface. The reported values of k_{3AMS}, k_{1ARM}, and magnetic inclinations are based on the present data set. Mgt = Magnetite grains.

In order to assess the influence of the speleothem's morphology on the recorded magnetic directions, SPAIV sample-based magnetic directions were compared with the dip angle of the corresponding calcite layers (Figure 4a). As already mentioned, the results show a striking linear correlation ($R^2 > 0.68$) between the recorded magnetic inclination and the dip of the calcite layer (Figure 4a): the steeper the calcite layer, the shallower the inclination of the NRM vector (Figure 6).

The inclination error observed in the studied speleothem can also be evidenced by comparing the present data with the SHA.DIF.14k geomagnetic field model [*Pavón-Carrasco et al.*, 2014]. The SHA.DIF.14K model is exclusively based on archaeomagnetic and lava flow data, and thus immune from possible influence of biased inclination data from sedimentary rocks. We analyzed the variation of the magnetic inclination of the speleothem under study between ~3970 years B.C. (line 13 on Figure 1) and 3430 years B.C. (line 3), and we considered the three following cases: (i) nearly vertical layers (column C + sample B5 on Figure 1), (ii) intermediate-steep (dip ~ 65–75°) layers (column I), and (iii) the top of the speleothem where calcite layer dip varies from 35° to 50° (column N). Results are illustrated in Figure 7. All lines show a trend comparable to the reference model within the interval of 3500–4000 years B.C.. The rate at which magnetic inclinations vary during this time interval is similar in the three cases (column B5-C, I, and N) and comparable to the characteristic increase of the Earth's magnetic field inclination observed in the SHA.DIF.14k model during the studied time-interval. This suggests that the remanent magnetization recorded by the speleothem is primary and provides a robust record of the Earth's magnetic field at the time of deposition. However, the magnetic inclinations from the speleothem are underestimated (below the 95% confidence interval) compared to the SHA.DIF.14K model and are gradually displaced from the reference curve as the calcite dip increases (Figure 7).

The speleothem investigated has no horizontal layer at the top, but since the relation between the remanent magnetic inclination and the calcite layer dip is linear (Figure 4a), we attempted to extrapolate the data to the horizontal (dip of 0° in Figure 4b). We first assume that the influence of the speleothem surface slope at any point should be the same for all lines, because calcite layers are mostly parallel in the speleothem under study (Figure 1). However, the linear regressions have slightly different slopes in Figure 4a, mostly due to measurement errors of the magnetic inclination (ex. line 11). For this reason, we calculate a mean variation rate of the

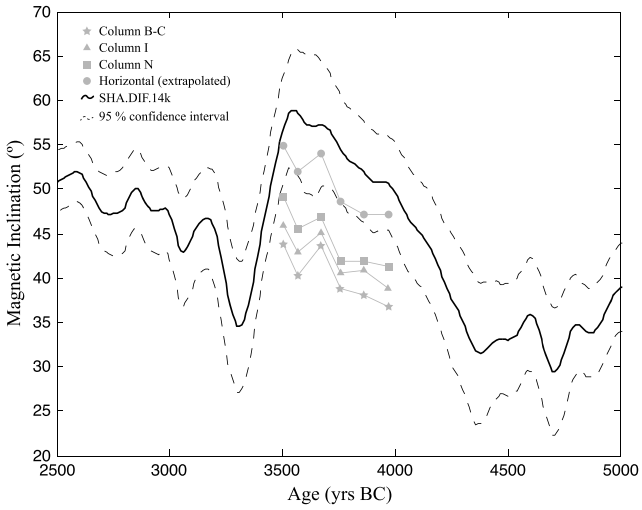

Figure 7. Comparison of the SPAIV magnetic inclinations with the SHA.DIF.14K model [*Pavón-Carrasco et al.*, 2014] calculated with respect to the speleothem age and for the cave's coordinates. The compared data refer to magnetic inclinations obtained from the samples in the column B and C (calcite dip angle ~75–85°), in column I (calcite dip angle ~65–75°), in column N (calcite dip angle ~35–50°), and extrapolated values to the horizontal layers (see text for more details).

magnetic inclination as a function of the speleothem surface slope based on all data (48 samples) (dashed line in Figures 4a and 4b). Subsequently, the trend line is anchored to the point defined by the sample-based mean magnetic inclination and mean calcite layer dip of each line (Figure 4b). With this approach, the influence of samples affected by measurement errors is minimized. The final extrapolated magnetic inclinations are obtained when considering a calcite dip layer value of 0°. Finally, we compared the extrapolated magnetic inclinations with the SHA.DIF.14K model to check for the validity of our approach. The resulting corrected PSV curve shows a better correlation with the SHA.DIF.14k model than original data (Figure 7). Inclination values are slightly lower than the mean inclinations given by the model but are within the 95% confidence envelope. These observations confirm our inference about the critical influence of the speleothem shape on the recorded magnetic inclinations and highlight the need to further investigate this effect in future studies on speleothem magnetism.

The process by which sediments (including speleothems) acquire a detrital remanent magnetization (DRM) is a very complex and not completely understood mechanism. Less is known in the case of speleothems [*Lascu and Feinberg*, 2011]. Paleomagnetic inclinations in sedimentary rocks are frequently suspected of being too shallow, and the recognition and correction of shallow bias have been the focus of numerous investigations [e.g., *Verosub*, 1977; *Tauxe and Kent*, 2004; *Tauxe et al.*, 2008]. Since the early 1950s, a number of laboratory experiments simulated the deposition of sediments in an attempt to investigate the origin of the inclination error observed in sediments (see *Bilardello* [2013] for a comprehensive review). Their results indicated that particle size and shape (anisotropy), gravity, viscosity, water current, surface slope angle, intensity and direction of the ambient magnetic field, and magnetic interactions between magnetic particles are the main factors controlling the acquisition of a DRM. Some inclination error also occurs during postdepositional remanent magnetization acquisition by processes of compaction, slumping, bioturbation, and water-filled voids allowing rotation of the magnetic minerals within the sediment matrix. However, such effects are insignificant in the case of speleothems, where burial and compaction are negligible, and where the time lag between the deposition of the magnetic particles and their immobilization by calcite precipitation is minimal [*Lascu and Feinberg*, 2011]. This leaves the ambient field, gravity, particle shape and size, slope, and magnetic interactions as the main possible factors controlling the acquisition of DRM in speleothems.

The influence of the shape and orientation of the magnetic grains along the speleothem surface were studied here by using AMS and AARM techniques. AMS experiments showed the presence of an oblate fabric, with k_3 varying from nearly horizontal to strongly dipping (~65°) depending on the location at the base or the top of the speleothem, respectively (Figure 6). However, it is not possible to unequivocally distinguish whether the AMS signal is controlled by calcite and/or by ferromagnetic particles. Previous studies of natural and synthetic calcite show that the fabric is dominantly oblate [*Schmidt et al.*, 2006; *Zhu et al.*, 2012]. In the case of speleothems having few or no detrital components, the k_3 is generally perpendicular to the speleothem surface and corresponds to the direction of the crystallographic axis of the calcite crystals [*Zhu et al.*, 2012]. In the present case, the speleothem has a significant amount of detrital material [*Font et al.*, 2014], as also observable by the reddish color of the speleothem. A significant amount of ferromagnetic grains is indicated by the

rather high values of the NRM (~10^{-3} A/m) (this study) and saturation isothermal remanent magnetization (SIRM ~ 10^{-1}–10^{-2} A/m [*Font et al.*, 2014]). However, the very low bulk susceptibility values, close to zero, strongly questioned the contribution of ferromagnetic minerals to the AMS signal. *Rochette* [1988] and *Schmidt et al.* [2006] observed that the AMS fabric changes from oblate to prolate when paramagnetic and/or ferromagnetic minerals are present, hence when their signal overcomes the negative susceptibility of calcite. In this case, the AMS fabric remains oblate independently of whether the K_m is positive or negative (Figure 5), suggesting that calcite is the main carrier of the AMS signal. This is consistent with the strong correlation of k_3 versus growth layer angle (R^2 = 0.95; Figure 4c). We thus conclude that the variations of k_3 are representative of the shape of the speleothem (i.e., of the slope of the growing surface) and not of the orientation of the ferromagnetic particles, similarly to what has been shown by *Zhu et al.* [2012].

AARM results differ strongly from those obtained by AMS techniques (Figure 5). AARM fabric presents a predominantly prolate shape (70% of the samples) with some samples having an oblate fabric (30%). The k_{1ARM} are relatively well clustered into the SE quadrant, and most samples exhibit a very low degree of anisotropy (P). Such difference in the fabrics reinforces the evidence that AARM is carried by significant amounts of ferromagnetic particles, while AMS is essentially controlled by calcite. The relatively low degree of anisotropy ($P < 1.114$) suggests a near-spherical shape of the magnetic minerals, typical of detrital magnetite grains. The fabric is preferentially prolate, with a minor contribution of oblate shapes. Inclination of the k_{1ARM} axes shows a significant correlation with the calcite layer dip (Figures 4d and 6). Independent of the shape (oblate or prolate) of the fabric, samples located at the top (vertical layers) of the speleothem show k_{1ARM} of ~70°, while samples located at the base (vertical layers) show k_{1ARM} ~ 40° (Figure 6). This suggests that (i) the particle shape has no or little control on the observed shallowing of the remanent inclination and (ii) the latter is indeed controlled by the orientation of the magnetic minerals along the speleothem surface.

The first point has been investigated by *King* [1955], *Griffiths et al.* [1960], and *Bilardello* [2013], who conducted deposition experiments with spherical and platy particles under different conditions. Contrarily to the model of *King* [1955], who proposed that inclination error is mostly due to platy magnetic particles that would flatten due to gravity and align with the horizontal surface, *Griffiths et al.* [1960] suggested that rolling of the spherical particles as they encounter the substrate could also generated shallow inclination. More recently, *Bilardello et al.* [2013] and *Bilardello* [2013] have shown that spheres alone may lead to significant amounts of shallowing and that this shallowing is also dependent on the ambient magnetic field.

Assuming that the particle shape has no influence on the shallowing of the inclination error, we suggest that the orientation of the magnetic particles along the surface of the speleothem under study is controlled by the interplay between the intensity/direction of the Earth's magnetic field during precipitation, gravity, and the slope of the speleothem surface. Gravity alone cannot explain the subsequent inclination errors, otherwise k_{1ARM} would be vertical (parallel to the slope) at the bottom of the speleothem, which is not the case (Figures 4d and 6). On the other hand, under the proviso that the magnetic inclinations provided by the SHA.DIF.14K are true, the direction of the Earth's magnetic field at the time of calcite precipitation alone cannot explain the observed remanent magnetic inclinations, which are ~5° lower in the extrapolated horizontal layer than in the SHA.DIF.14K model (Figure 7). This scenario (i.e., the case of the horizontal layer) is comparable to the experiment of *Bilardello et al.* [2013], who conducted a laboratory experiment using spherical magnetic grains settled in a tube. Considering field inclination of 30° and 60°, the authors obtained inclination shallowing of 7–20°, values compatible to our case study. Based on a newly developed numerical model, *Bilardello et al.* [2013] also suggested that particle collision during settling combined with both rolling and slipping (translation) is consistent with the experimental results. This model would also explain why the orientations of the magnetic particles evidenced by the orientation of k_{1ARM} are much more scattered at the bottom of the speleothem than the top. As gravity preferentially acts on the subvertical slope at the bottom and/or the ferromagnetic grains roll more because of the increased travel distance, the directions of k_{1ARM} become more scattered and shallow [*Jezek et al.*, 2012; *Bilardello et al.*, 2013].

These findings are illustrated in Figure 6. Note that the difference observed between the magnetic inclination measured at the bottom and the top of the speleothem differ from ~5°, whereas the difference observed between the k_{1ARM} is more than 30°. This corroborates the observation of *Jackson et al.* [1991], who suggested that the orientation of the long axes of the ferromagnetic particles is mainly controlled by physical mechanism (rolling in this case), while the orientation of the magnetic moment is mainly controlled by the

geomagnetic field. The increased misalignment of the magnetic particles results in a net distribution of magnetic moments that is shallower than the orientation of the ambient geomagnetic field.

Although our findings are specific to the speleothem investigated, whose shape is not common, it provides important insights into the NRM acquisition mechanisms in speleothems. Accordingly, it is also strongly recommended to study horizontal layers collected in the center of the speleothems, in agreement to what has been done in recent paleomagnetic studies [e.g., *Osete et al.*, 2012; *Lascu et al.*, 2016], where shallowing effect is suggested to be minor. However, further investigations are urgently needed to evaluate the extent of the shallow inclinations and improve the representativeness of paleomagnetic data in speleothems.

6. Conclusions

Our results show that the recorded magnetic inclinations in the speleothem under investigation are strongly influenced by its shape. Comparing the obtained magnetic inclinations with a global paleosecular variation model (PSV) indicates that magnetic inclinations move gradually away from the PSV curve as the surface slope increases. The best fit between our data and the PSV model is obtained when extrapolating magnetic inclinations to the horizontal.

Although the studied speleothem contains significant amounts of detrital particles (including ferromagnetic grains), its AMS signal is dominantly carried by diamagnetic calcite, attested by negative bulk magnetic susceptibility, and corresponds to an oblate fabric where k_3 represents the crystallographic direction of the calcite growths and thus mimics the shape of the speleothem. On the other hand, the orientation of the AARM ellipsoid is perpendicular to the calcite layers and its orientation varies according to the slope of the layers; i.e., the steeper the slope, the shallower the k_{1ARM}. Although the remanent magnetic directions recorded in the speleothem under study are mainly controlled by the ambient geomagnetic field, inclination error may result from the influence of physical mechanism, such as particle rolling and slipping during transport along the slope. Increased misalignment of the ferromagnetic particles results in a net distribution of directions that is shallower than that of the ambient geomagnetic field. Contrarily to previous studies suggesting that speleothem shapes had no influence on the remanent magnetization, the present data provide the first and undisputable piece of evidence against this conclusion. Our data also suggest that inclination error may occur even in horizontal layers, and this aspect should deserve more attention in forthcoming paleomagnetic studies of speleothems.

Acknowledgments

Funding was provided by the Institute Dom Luis (FCT UID/GEO/50019/2013), University of Lisbon, by the Portuguese government and through the FCT-Fundação para a Ciência. This work was performed as part of the PhD of Jorge Ponte (Instituto Dom Luís, Universidade de Lisboa) granted by FCT (SFRH/BD/96241/2013). We thank Celia Lee for administrative support. We are grateful to the regional speleology association (CEEAA) for their help during the sampling of the speleothem, Martin Chadima for helping with AARM analysis, Marta Neres and Pedro Silva for discussion, and Dario Bilardello for giving precious insight, advice about inclination error, and for proofreading the manuscript. We thank Joshua Feinberg, an anonymous reviewer, and the Associate Editor Mark Dekkers for their fruitful comments, which helped us improve the quality of our manuscript. The data for this paper are available by contacting the corresponding author (e-mail: jorgeponte89@gmail.com).

References

Bilardello, D. (2013), Understanding DRM acquisition of plates and spheres: A first comparative experimental approach, *Geophys. J. Int.*, *195*, 148–158.

Bilardello, D., J. Jezek, and S. A. Gilder (2013), Role of spherical particles on magnetic field recording in sediments: Experimental and numerical results, *Phys. Earth Planet. Inter.*, *214*, 1–13.

Bourne, M. D., J. M. Feinberg, B. E. Strauss, B. Hardt, H. Cheng, H. D. Rowe, G. Springer, and R. L. Edwards (2015), Long-term changes in precipitation recorded by magnetic minerals in speleothems, *Geology*, *43*, 595–598.

Borradaile, G. J., and M. Jackson (2010), Structural geology, petrofabrics and magnetic fabrics (AMS, AARM, AIRM), *J. Struct. Geol.*, *32*, 1519–1551, doi:10.1016/j.jsg.2009.09.006.

Fisher, R. (1953), Dispersion on a sphere, *Proc. R. Soc. A*, *217*(1130), 295–305.

Font, E., C. Veiga-Pires, M. Pozo, C. Carvallo, A. C. Siqueira Neto, P. Camps, S. Fabre, and J. Mirão (2014), Magnetic fingerprint of southern Portuguese speleothems and implications for paleomagnetism and environmental magnetism, *J. Geophys. Res. Solid Earth*, *119*, 7993–8020, doi:10.1002/2014JB011381.

Ghaleb, B., C. Veiga-Pires, D. Moura, and C. Hillaire-Marcel (2014), Multi-proxy constraints on ages of low U-content, young and "dirty" speleothems: Example from southern Portugal cave deposits, Abstract presented at EGU, Wien, Austria.

Griffiths, D. H., R. F. King, A. I. Rees, and A. E. Wright (1960), The remanent magnetism of some recent varved sediments, *Proc. R. Soc. London, Ser. A.*, *256*, 359–383.

Hellstrom, J. (2006), U-Th dating of speleothems with high initial ^{230}Th using stratigraphical constraint, *Quat. Geochronol.*, *1*, 289–295.

Hill, C., and P. Forti (1997), *Cave Minerals of the World*, *Natl. Speleol. Soc.*, 2nd ed., 463 pp. Huntsville, Ala.

Hirt, A. H., and B. S. G. Almqvist (2012), Unraveling magnetic fabrics, *Int. J. Earth Sci. (Geol. Rundsch)*, *101*, 613–624, doi:10.1007/s00531-011-0664-0.

Hrouda, F. (1986), The effect of quartz on the magnetic anisotropy of quartzite, *Stud. Geophys. Geod.*, *30*(1), 39–45.

Jackson, M. J., S. K. Banarjee, J. A. Marvin, R. Lu, and W. Gruber (1991), Detrital remanence, inclination errors, and anhysteretic remanence anisotropy: Quantitative model and experimental results, *Geophys. J. Int.*, *104*, 95–103.

Jaqueto, P., R. Trindade, G. Hartmann, V. Novello, F. Cruz, I. Karmann, B. Strauss, and J. Feinberg (2016), Linking speleothems and soil magnetism in the Pau d' Alho cave (Central South America), *J. Geophys. Res. Solid Earth*, *121*, 7024–7039, doi:10.1002/2016JB013541.

Jelinek, V. (1981), Characterization of the magnetic fabric of rocks, *Tectonophysics*, *79*, 63–67.

Jezek, J., S. A. Gilder, and D. Bilardello (2012), Numerical simulation of inclination shallowing by rolling and slipping of spherical particles, *Comput. Geosci.*, *49*, 270–277.

King, R. F. (1955), The remanent magnetism of artificially deposited sediments, *Geophys. J. Int.*, *7*, 115–134.
Kirschvink, J. L. (1980), The least-squares line and plane and the analysis of palaeomagnetic data, *Geophys. J. R. Astron. Soc.*, *62*(3), 699–718.
Lascu, I., and J. M. Feinberg (2011), Speleothem magnetism, *Quat. Sci. Rev.*, *30*, 3306–3320, doi:10.1016/j.quascirev.2011.08.004.
Lascu, I., J. M. Feinberg, J. M. Dorale, H. Cheng, and R. L. Edwards (2016), Age of the Laschamp excursion determined by U-Th dating of a speleothem geomagnetic record from North America, *Geology*, *44*, 139–142.
Latham, A. G., H. P. Schwarcz, D. C. Ford, and G. W. Pearce (1979), Paleomagnetism of speleothem deposits, *Nature*, *280*, 383–385.
Latham, A. G., H. P. Schwarcz, D. C. Ford, and G. W. Pearce (1982), The paleomagnetism and U-Th dating of three Canadian speleothems: Evidence for the westward drift, 5.4–2.1 ka BP, *Can. J. Earth Sci.*, *19*, 1985–1995.
Latham, A. G., H. P. Schwarcz, and D. C. Ford (1986), The paleomagnetism and U-Th dating of Mexican speleothem, *Earth Planet. Sci. Lett.*, *79*, 195–207.
Latham, A. G., D. C. Ford, H. P. Schwarcz, and T. Birchall (1989), Secular variation from Mexican speleothems: Their potential and problems, *Phys. Earth Planet. Inter.*, *56*, 34–48.
Lean, C. B., A. G. Latham, and J. Shaw (1995), Palaeosecular variation from a Vancouver Island speleothem and comparison with contemporary North American records, *J. Geomagn. Geoelectr.*, *47*, 71–87.
Martin, K. (1990), Paleomagnetism of speleothems in Gardner cave, Washington, *Natl. Speleol. Soc. Bull.*, *52*, 87–94.
McCabe, C., M. Jackson, and B. B. Ellwood (1985), Magnetic anisotropy in the Trenton limestone: Results of a new technique, anisotropy of anhysteretic susceptibility, *Geophys. Res. Lett.*, *12*, 333–336, doi:10.1029/GL012i006p00333.
Morinaga, H., H. Inokuchi, and K. Yaskawa (1986), Magnetization of a speleothem in Akiyoshi Plateau as a record of the geomagnetic secular variation in West Japan, *J. Geomagn. Geoelectr.*, *38*, 27–44.
Morinaga, H., H. Inokuchi, and K. Yaskawa (1989), Palaeomagnetism of speleothems (speleothems) in SW Japan, *Geophys. J.*, *96*, 519–528.
Openshaw, S., A. Latham, and J. Shaw (1997), Speleothem palaeosecular variation records from China; their contribution to the coverage of Holocene palaeosecular variation data in East Asia: Paleosecular variation and intensity, *J. Geomagn. Geoelectr.*, *49*, 485–505.
Osete, M. L., J. Martin-Chivelet, C. Rossi, R. L. Edwards, R. Egli, M. B. Munoz-Garcia, X. F. Wang, F. J. Pavon-Carrasco, and F. Heller (2012), The Blake geomagnetic excursion recorded in a radiometrically dated speleothem, Earth Planet, *Sci. Lett.*, *353*, 173–181.
Pavón-Carrasco, F. J., M. L. Osete, J. M. Torta, and A. De Sanctis (2014), A geomagnetic field model for the Holocene based on archaeomagnetic and lava flow data, *Earth Planet. Sci. Lett.*, *388*, 98–109.
Rochette, P. (1988), Inverse magnetic fabric in carbonate-bearing rocks, *Earth Planet. Sci. Lett.*, *90*, 229–237, doi:10.1016/0012-821X(88)90103-3.
Schmidt, V., D. Gunther, and A. M. Hirt (2006), Magnetic anisotropy of calcite at room-temperature, *Tectonophysics*, *418*, 63–73.
Scholz, D., and D. L. Hoffmann (2011), An algorithm designed for construction of speleothem age models, *Quat. Geochronol.*, *6*, 369–382.
Strauss, B. E., J. H. Strehlau, I. Lascu, J. A. Dorale, R. L. Penn, and J. M. Feinberg (2013), The origin of magnetic remanence in speleothems: Observations from electron microscopy and rock magnetism, *Geochem. Geophys. Geosyst.*, *14*, 5006–5025, doi:10.1002/2013GC004950.
Tarling, D. H., and F. Hrouda (1993), *The Magnetic Anisotropy of Rocks*, 227 pp., Chapman and Hall, London.
Tauxe, L., and D. V. Kent (2004), A simplified statistical model for the geomagnetic field and the detection of shallow bias in paleomagnetic inclinations: Was the ancient magnetic field dipolar?, in *Timescales of the Paleomagnetic Field*, edited by J. E. T. Channell et al., pp. 101–115, AGU, Washington, D. C., doi:10.1029/145GM08.
Tauxe, L., K. P. Kodama, and D. V. Kent (2008), Testing corrections for paleomagnetic inclination error in sedimentary rocks: a comparative approach, *Phys. Earth Planet. Inter.*, *169*, 152–165.
Terrinha, P., et al. (2013), A Bacia do Algarve: Estratigrafia, paleogeografia e tectónica, in *Geologia de Portugal, Vol. II: Geologia Meso-cenozóica de Portugal*, edited by R. Dias et al., pp. 29–166, Livraria Escolar Editora, Lisboa.Cap. III.1.
Veiga-Pires, C., B. Ghaleb, J. Hélie, D. Moura, J. Luis, and C. Hillaire-Marcel (2011), A first Last Glacial Maximum to Younger Dryas stalagmite record from southern Portugal, Geophysical Research Abstracts, EGU 2011, 13.
Verosub, K. L. (1977), Depositional and postdepositional processes in the magnetization of sediments, *Rev. Geophys. Space Phys.*, *15*(2), 129–143.
Zhu, Z. M., S. H. Zhang, C. Y. Tang, H. Y. Li, S. C. Xie, J. L. Ji, and G. Q. Xiao (2012), Magnetic fabric of speleothems and its formation mechanism, *Geochem. Geophys. Geosyst.*, *13*, Q06006, doi:10.1029/2011GC003869.